

CHANDRA EVIDENCE FOR AGN FEEDBACK IN THE SPIRAL GALAXY NGC 6764

J.H. CROSTON¹, M.J. HARDCASTLE¹, P. KHARB², R.P. KRAFT³, A. HOTA⁴

Draft of October 20, 2021

ABSTRACT

We report the *Chandra* detection of X-ray emission spatially coincident with the kpc-scale radio bubbles in the nearby ($D_L \sim 31$ Mpc) AGN-starburst galaxy NGC 6764. The X-ray emission originates in hot gas ($kT \sim 0.75$ keV), which may either be contained within the radio bubbles, or in a shell of hot gas surrounding them. We consider three models for the origin of the hot gas: (1) a starburst-driven galactic wind, (2) shocked gas associated with the expanding radio bubbles, and (3) gas heated and entrained into the bubbles by jet/ISM interactions in the inner AGN outflow. We rule out a galactic wind based on significant differences from known galactic wind systems. The tight correspondence between the brightest X-ray emission and the radio emission in the inner outflow from the Seyfert nucleus, as well as a correlation between X-ray and radio spectral features suggestive of shocks and particle acceleration, lead us to favour the third model; however, we cannot firmly rule out a model in which the bubbles are driving large-scale shocks into the galaxy ISM. In either AGN-driven heating scenario, the total energy stored in the hot gas is high, $\sim 10^{56}$ ergs, comparable to the energetic impact of low-power radio galaxies such as Centaurus A, and will have a dramatic impact on the galaxy and its surroundings.

Subject headings: galaxies: active – X-rays: galaxies

1. INTRODUCTION

Galaxy feedback processes are now thought to be an important ingredient in galaxy formation models (e.g. Croton et al. 2006; Bower et al. 2006), potentially solving the long-standing problem of explaining the deficit of galaxies at the low and high mass ends of the galaxy luminosity function relative to model predictions. Disentangling the feedback contributions from AGN outbursts and from star formation to the energetics of gas in galaxies, galaxy groups and clusters is a key problem in galaxy evolution, as it is clear that both can inject large quantities of energy into their surroundings. While there is growing evidence that AGN outbursts are the dominant feedback process operating at the high-mass end of the galaxy luminosity function, it might be expected that at lower masses, and particularly in late-type galaxies, the energy input from star formation processes will dominate.

Recent work has shown that kpc-scale radio bubbles connected to an active nucleus can be found in many Seyfert galaxies (e.g. Gallimore et al. 2006; Kharb et al. 2006). Although it has been argued that these bubbles may be powered by stellar winds (e.g. Baum et al. 1993), the fact that no convincing examples exist in galaxies without an AGN strongly suggests that they are inflated by the active nucleus (e.g. Hota & Saikia 2006, hereafter HS06). Many of the known Seyfert radio bubbles are predicted to be overpressured with respect to their surroundings (e.g. Capetti et al. 1999), and therefore may be shocking the surrounding medium, as has been observed for kpc-scale radio lobes in massive elliptical galaxies (e.g. Centaurus A: Kraft et al. 2003; NGC 3801: Croston et al. 2007).

In order to search for evidence for galaxy feedback as-

sociated with kpc-scale radio bubbles in spiral galaxies, we carried out a *Chandra* observation of the nearby Seyfert 2/LINER galaxy NGC 6764, which is a barred spiral galaxy (type SB(s)bc) with non-thermal radio bubbles perpendicular to the plane of the galaxy disk that extend for ~ 1 kpc (Fig. 1). Here we report on the results of this observation.

Throughout this paper, we adopt a cosmology with $H_0 = 70$ km s⁻¹ Mpc⁻¹, $\Omega_M = 0.3$ and $\Omega_\Lambda = 0.7$. We adopt a luminosity distance for NGC 6764 of 31.3 Mpc, obtained by correcting the heliocentric velocity of 2146 km s⁻¹ to the CMB frame of reference. This gives an angular scale of $1'' = 0.15$ kpc at the distance of NGC 6764.

2. DATA ANALYSIS

We observed NGC 6764 with *Chandra* (ACIS-S) for 20 ks on 2008 January 20th. The observation was taken in VFaint mode to minimize the background level. The data were reprocessed from the level 1 events file with CIAO 3.4 and CALDB 3.4.2, including VFaint cleaning. The latest gain files were applied and the 0.5-pixel randomization removed using standard techniques detailed in the CIAO on-line documentation⁵. An inspection of the lightcurve for our observation using the *analyze_ltcrv* script showed that there were no periods of high background level, and so no additional GTI filtering was applied.

We produced a 0.5 – 5 keV filtered image to examine the X-ray emission associated with the galaxy, presented in Fig. 2. The most prominent feature in the image is the region of extended emission, which is located exactly coincident with the bubbles of radio emission shown in the right hand panel. In addition, there is a region of brighter X-ray emission in the centre of the emitting region on scales of $\sim 4''$, coincident with the AGN and extending to the west, while becoming broader. This bright region coincides with a region of higher surface brightness radio emission, as shown in the higher resolution 5-GHz radio map in Fig. 11 of HS06.

We extracted spectra from the Seyfert nucleus, the bright

¹ School of Physics, Astronomy and Mathematics, University of Hertfordshire, College Lane, Hatfield AL10 9AB, UK

² Department of Physics, Purdue University, 525 Northwestern Avenue, West Lafayette, IN 47907, USA

³ Harvard-Smithsonian Center for Astrophysics, 60 Garden Street, Cambridge, MA 02138, USA

⁴ Institute of Astronomy and Astrophysics, Academia Sinica, P.O. Box 23-141, Taipei 10617, Taiwan, R.O.C.

⁵ <http://asc.harvard.edu/ciao/>

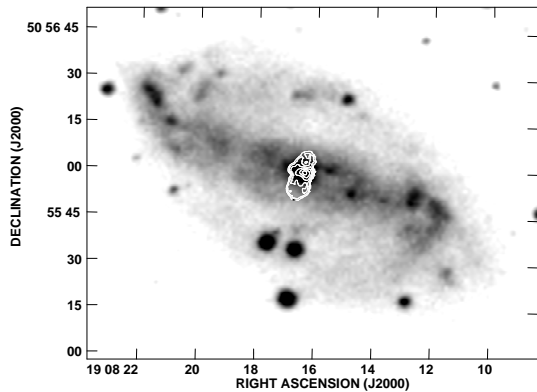


FIG. 1.— 1.4-GHz radio contours of NGC 6764 overlaid on a DSS-2 optical image of the host galaxy. The radio map is made from VLA archival data as published in Hota & Saikia (2006). Contour levels are $(1.5 \times 10^{-4}) \times 1, 2, 4, \dots, 512$ Jy beam $^{-1}$.

central region, the two lobes (both separately and together to improve the signal-to-noise ratio) and from a large region encompassing the galaxy disk, using the *specextract* script, which also builds the appropriate response files. Local background regions adjacent to or surrounding the source extraction regions were used. Spectra were grouped to 20 counts per bin after background subtraction prior to spectral fitting, which was carried out using *XSPEC*. We assumed a fixed Galactic absorption of $N_H = 6.0 \times 10^{20}$ cm $^{-2}$ in our spectral fitting (Dickey & Lockman 1990), except where otherwise specified.

3. RESULTS

3.1. Radio-related X-ray emission

We measure a total of ~ 1150 net 0.5 – 5 keV ACIS-S counts from the regions coincident with the radio bubbles (excluding the bright central region). In what follows we will refer to these X-ray emitting regions as “X-ray bubbles” for simplicity but without any implied geometry for the emitting fluid. We fitted a series of models to the bubble spectra to distinguish between different origins for the X-ray emission. We initially considered the spectrum for the entirety of the bubble regions, using a local background region (source and background extraction regions are shown in Fig. 2). We fitted both single power law and single *mekal* model (with Galactic absorption, as described above, and free abundance for the thermal model). The power-law model gave an unacceptable fitting statistic ($\chi^2 = 181$ for 25 d.o.f.), and allowing the value of Galactic column density to vary as a proxy for any absorption intrinsic to the galaxy did not allow an acceptable fit to be obtained. We obtained a good fit with the *mekal* model, with best-fitting values of $kT = 0.75 \pm 0.05$ keV and $Z = 0.13^{+0.05}_{-0.03} Z_\odot$ and $\chi^2 = 25.5$ for 24 d.o.f. This model fit is shown in Fig. 3. Allowing the total absorbing column to vary to account for any intrinsic absorption does not significantly change the best-fitting temperature or abundance values (although the total absorbing column density was left free, it did not fall below the assumed Galactic column). We note that the low abundance values may be due to fitting a single-temperature model to a multi-temperature plasma (e.g. Buote et al. 2000), and so are likely to be unreliable. Given the very poor fitting statistics obtained for a single power-law model, we can firmly rule out a non-thermal origin for the X-ray emission associated with the radio bub-

bles. We added a power-law component to the spectrum to investigate whether some contribution from non-thermal emission is present; however, this did not significantly affect the fit statistic or the parameters of the *mekal* component. While we cannot rule out some contribution from non-thermal emission, the X-ray emission predominantly originates from gas of $kT \sim 0.75$ keV. We measure a total, unabsorbed 0.5 – 2.0 keV flux from the X-ray bubbles of 1.2×10^{-13} erg cm $^{-2}$ s $^{-1}$, corresponding to a luminosity of $\sim 1.4 \times 10^{40}$ erg s $^{-1}$.

To investigate whether there is any spatial variation in the properties of the X-ray-emitting gas, we examined spectra of the regions corresponding to the northern and southern bubbles separately. The properties of the two bubbles appear to be fairly similar both to each other and to the results for the joint spectrum discussed above. In neither case is a power-law model an adequate fit (either with fixed or free N_H), and in both cases good fits could be obtained with a single *mekal* model. For the northern bubble we obtained a best-fitting temperature of $kT = 0.81^{+0.08}_{-0.07}$ keV and $Z = 0.14^{+0.09}_{-0.05} Z_\odot$ with $\chi^2 = 10.3$ for 9 d.o.f., and for the southern bubble we obtained a best-fitting temperature of $kT = 0.64^{+0.06}_{-0.05}$ keV and $Z = 0.12^{+0.06}_{-0.04} Z_\odot$ with $\chi^2 = 15.9$ for 13 d.o.f. Therefore there is a small, but statistically significant difference in the temperatures of the two bubbles, with the southern bubble slightly cooler than the northern one. The origin of this small difference is unclear, but could be related to differences in the distribution of material being heated in the north and south.

Finally, we also examined the spectrum of the brighter central region of X-ray emission (Fig. 5; 2–4'' scales) in the same way. We found that for this emission neither a *mekal* nor a power-law model gave an acceptable fit if Galactic absorption was assumed; however, an acceptable fit could be obtained for a *mekal* model if the value of N_H was permitted to vary (again we varied the overall column density, but it did not drop below the assumed Galactic value). We obtained a good fit with $N_H = (2.0^{+1.5}_{-0.7}) \times 10^{21}$ cm $^{-2}$, $kT = 0.93^{+0.12}_{-0.18}$ keV, and abundance fixed at the value measured for the outer regions, with $\chi^2 = 16.7$ for 12 d.o.f. If the abundance is fixed at solar abundance, we find a best fit with $N_H = (7.7^{+1.3}_{-1.0}) \times 10^{21}$ cm $^{-2}$ and $kT = 0.65^{+0.22}_{-0.11}$ keV, with $\chi^2 = 18.3$ for 12 d.o.f. A power-law model with free N_H did not give an acceptable fit, and so we conclude that the brighter central X-ray emission also has a thermal origin. The temperature of this gas is consistent with that in the regions associated with the radio bubbles.

3.2. The Seyfert nucleus

We extracted a spectrum from a 1.5'' radius circle centred on the Seyfert nucleus, which we assumed to be located at the peak of the X-ray emission. This position is in agreement with the position of the Seyfert nucleus determined from optical observations (Clements 1981) to within the accuracy of *Chandra*'s astrometry. We found that single power-law models were unacceptable whether the overall absorption was fixed at the Galactic value or left as a free parameter as a proxy for a contribution from intrinsic absorption. A single *mekal* model was also unacceptable with either Galactic or free absorption. We therefore fitted a model consisting of a *mekal* component plus an intrinsically absorbed power law. Since the number of spectral bins is fairly low, the power-law index was fixed at $\Gamma = 1.5$, a typical value for nuclear emission (a steeper value, e.g. $\Gamma = 2.0$, does not significantly alter the results). We obtained a good fit for this model, with $\chi^2 = 10.1$ for 7 d.o.f.,

FIG. 2. — Left: 0.5 - 5.0 keV image of the *Chandra* data, smoothed with a Gaussian of $0.6''$ FWHM, showing emission associated with the radio bubbles; right: X-ray emission in colour smoothed with a Gaussian of $1.8''$ FWHM, with radio contours overlaid. Contour levels are as for Fig. 1.

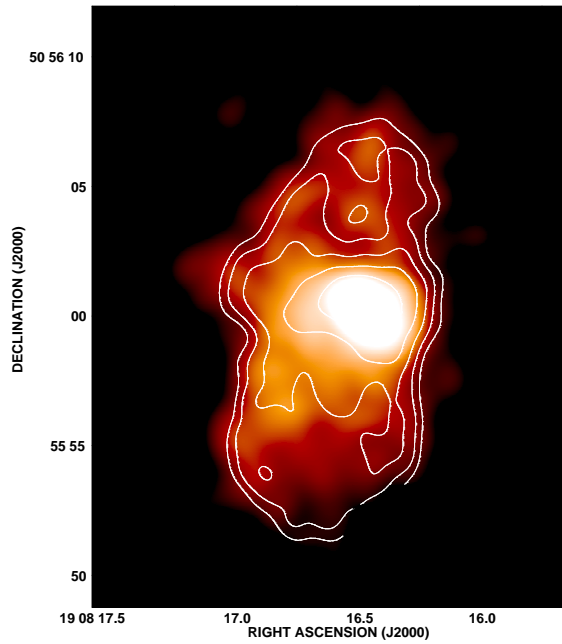
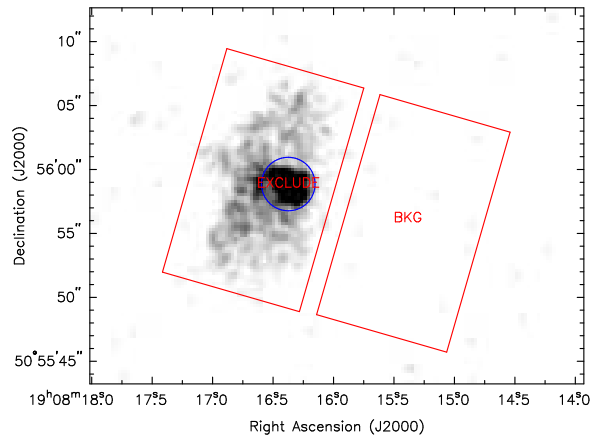
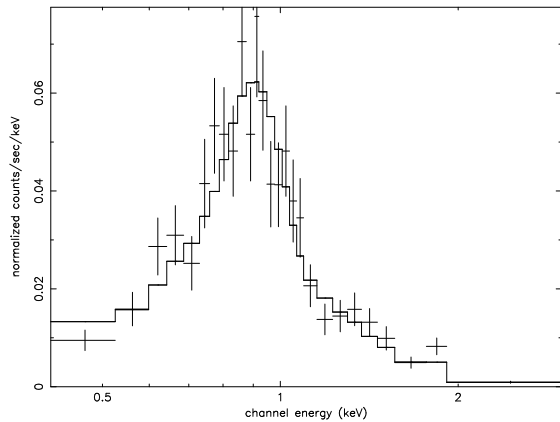


FIG. 3. — ACIS-S counts spectrum for the entire bubble region in the energy range 0.4 - 7.0 keV, with best-fitting *mekal* model, as described in the text, overlotted.



$kT = 0.92^{+0.16}_{-0.05}$ keV, and $N_H = (2.9^{+3.6}_{-1.8}) \times 10^{21}$ cm $^{-2}$. For this best-fitting model, we obtained an unabsorbed 2.0 - 10.0 keV flux for the power-law component of $(3.4^{+1.0}_{-1.2}) \times 10^{-14}$ ergs cm $^{-2}$ s $^{-1}$, which corresponds to a 1-keV flux density of $4.0^{+1.1}_{-1.4}$ nJy and implies a 2.0 - 10.0 keV unabsorbed nuclear luminosity of $(4.0^{+1.2}_{-1.4}) \times 10^{39}$ ergs s $^{-1}$. The uncertainties here take account of the large uncertainty in the absorbing column. The unabsorbed 0.5 - 2.0 keV flux of the thermal component is $(3.0^{+0.6}_{-0.5}) \times 10^{-14}$ ergs cm $^{-2}$ s $^{-1}$, corresponding to a luminosity of $(3.5^{+0.8}_{-0.6}) \times 10^{39}$ ergs s $^{-1}$. The total unabsorbed nuclear 2.0 - 10.0 keV luminosity is $\sim 4.4 \times 10^{39}$ ergs s $^{-1}$.

It is common for type 2 Seyfert nuclei to have strong intrinsic absorption, artificially lowering the inferred X-ray luminosity [e.g. Awaki et al. (2000), Terashima & Wilson (2001), Matt et al. (2004), Matsumoto et al. (2004)]. A more conservative upper limit can be obtained by assuming a typical value

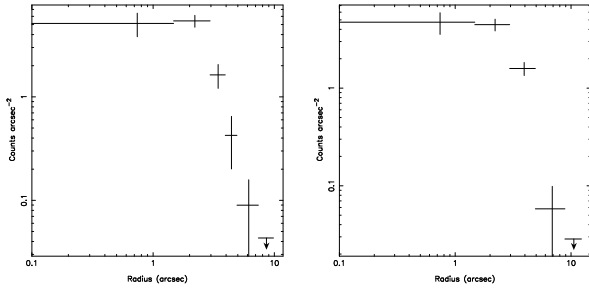
of the intrinsic absorption for Seyfert 2s where detailed X-ray analysis is available. We therefore also fitted a model with a *mekal* plus heavily absorbed power law, with $N_H = 3 \times 10^{23}$ cm $^{-2}$ [the value measured for the Seyfert 2 M51 by Terashima & Wilson (2001)] in order to determine a conservative upper limit on the intrinsic nuclear luminosity. Fixing the power-law normalisation at the upper limit allowed by the best-fitting model, we found that the data are consistent with a heavily obscured power-law component with a 2.0-10.0 keV luminosity as high as $\sim 2 \times 10^{41}$ erg s $^{-1}$. Hence we cannot rule out the presence of an intrinsically bright nucleus that is heavily obscured.

4. ENERGETICS OF THE X-RAY-EMITTING GAS AND RADIO BUBBLES

As shown in Fig. 2, the X-ray emission appears to trace the 1.4-GHz radio structure in NGC 6764 very closely. There is evidence for a surface-brightness deficit in both the X-ray and radio emission in the centre of the northern bubble, and to a lesser extent in the centre of the southern bubble; however, the X-ray structure is not strongly edge-brightened as seen in shocked shells surrounding the kpc-scale lobes of radio galaxies (e.g. Kraft et al. 2003; Croston et al. 2007). We cannot distinguish between a model where the hot gas is inside the radio bubbles and one where it is in shell structures surrounding them based on the X-ray morphology alone.

To investigate the energetics of the bubbles we therefore considered two possible scenarios: (1) the X-ray-emitting gas fills the radio bubbles, (2) the X-ray-emitting gas is located in shells surrounding the radio bubbles. Based on the outer extent of the X-ray emission from the southern bubble (which has a more spherical appearance), we assumed an outer radius for the emitting region of $4.2''$, which corresponds to 0.7 kpc. For scenario (1) we assumed a sphere of this radius, and for scenario (2) we assumed a spherical shell with thickness 0.1 kpc. Assuming a constant density and a filling factor of unity in the emitting region, these geometries lead to inferred

FIG. 4.— Surface brightness profiles for the northern (l) and southern (r) bubbles obtained in a slice towards the bubble edge. Centre of the profile is the bubble centre in each case (not the galaxy nucleus).



electron densities of 0.19 cm^{-3} and 0.30 cm^{-3} , for scenarios 1 and 2, respectively. For the measured temperature of the southern bubble X-ray emission, these correspond to pressures of $(4 - 7) \times 10^{-12} \text{ dyne cm}^{-2}$. For the northern bubble, we assumed an outer radius of $4.0''$, and the same shell thickness for scenario 2, which led to inferred electron densities of 0.17 cm^{-3} and 0.27 cm^{-3} for scenarios 1 and 2, respectively, and to pressures consistent with those of the southern bubble. For lower filling factors, the gas densities (and pressures as inferred below) will increase. The total gas mass is $\sim 10^7 M_{\odot}$, a small fraction of the ISM mass likely to be contained in the galaxy's bulge.

We determined the equipartition internal pressures of the two bubbles using measurements of the 1.4-GHz flux density for each lobe to normalize the synchrotron spectrum. We assumed a filling factor of unity, a broken power-law electron distribution with initial electron energy index, δ , of 2.1, $\gamma_{\text{min}} = 10$ and $\gamma_{\text{max}} = 10^5$, and a break at $\gamma_{\text{break}} = 10^3$, and modelled the lobes as spheres of radius 4.0 and $4.2''$, respectively, for the northern and southern bubbles. The resulting equipartition internal pressures were $\sim 1.2 \times 10^{-13} \text{ dyne cm}^{-2}$ for both bubbles, which are a factor of $\sim 30 - 50$ times lower than the pressure in the hot gas. Hence if the hot gas is external to the radio bubbles, an additional source of pressure in the bubbles is required to balance that in the hot gas. However, it is known that external pressures from hot gas surrounding most low-power radio-galaxy lobes are significantly higher than internal equipartition pressures (e.g. Morganti et al. 1988; Croston et al. 2003, 2008), and so this is not on its own a strong argument against the gas being outside the radio bubbles. In particular, the external pressures of the shocked shells in NGC 3801 and Centaurus A (Croston et al. 2007; Kraft et al. 2003) are factors of ~ 70 and ~ 15 times higher, respectively, than the internal equipartition radio-lobe pressures.

Based on the two scenarios for the geometry of the X-ray-emitting material discussed above, we determined the total thermal energy stored in the hot gas to be $(3 - 5) \times 10^{55}$ ergs, which is comparable to the energy stored in the shocked shells surrounding the lobes of the radio galaxy NGC 3801 ($\sim 8 \times 10^{55}$ ergs).

We also determined the physical properties of the central region of brighter, thermal X-ray emission. As shown in Fig. 5, this region corresponds closely to a brighter region of radio emission. The narrowest part of the brighter region coincides with the position of the Seyfert nucleus, leading HS06 to interpret this emission as a radio jet oriented towards the western edge of the large-scale radio bubbles. The X-ray and radio emission from this brighter region corresponds very closely, and it has the appearance of a poorly collimated outflow. If this is indeed an outflow, then it is likely to be supplying ma-

terial to the large-scale bubbles. We therefore also investigated the energetics of this inner region. Assuming a spherical region of radius $1.85''$, we find an electron density between $0.76 - 0.80 \text{ cm}^{-3}$ corresponding to a gas pressure of $(8.3 - 11) \times 10^{-12} \text{ dyne cm}^{-2}$ (the ranges given here take into account a range in metallicity from $[0.15 - 1]Z_{\odot}$). Hence the inner gas is overpressured by as much as a factor two relative to the outer X-ray bubbles, and should be expanding and possibly heating the outer gas through weak shocks. It is also possible that the radio bubble is providing pressure support for this higher pressure gas, or that the gas is being compressed by the expanding radio bubble. We discuss the implications of this expanding hot gas in the centre of the galaxy, and its relation to the larger X-ray bubbles in the sections that follow.

5. ORIGIN OF THE X-RAY EMISSION: GALACTIC WIND OR JET-DRIVEN SHOCKS?

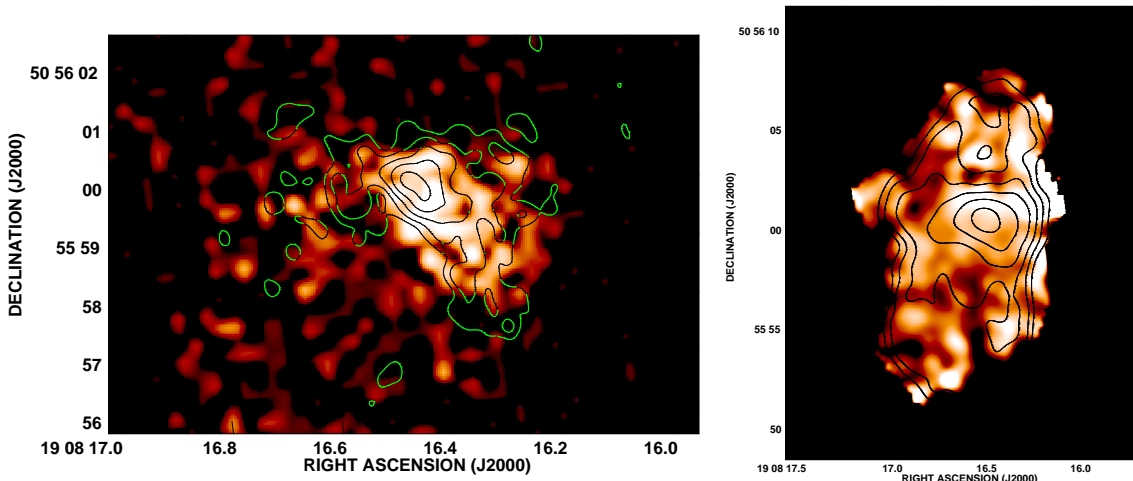
The two most likely explanations for the origin of the X-ray emission in NGC 6764 are: (I) hot gas in a galactic wind, similar to the X-ray emission seen in typical nearby starburst galaxies, or (II) emission from material that has been heated by the expanding radio plasma. However, there are some clear problems with both scenarios, as neither can fully explain the very tight correspondence between radio and X-ray morphology. A third possibility, suggested by this correspondence, is that both the radio and X-ray emission are produced by the same particles. However, the steep radio spectral index of the bubbles is not consistent with a thermal origin for the radio emission, and the X-ray spectra of the bubbles are clearly inconsistent with a non-thermal origin. The observed flux level is also much higher than would be predicted by an inverse-Compton model, so that this model can be firmly ruled out. Therefore, we can find no obvious explanation in which the X-ray emission is produced by the same particles as the radio emission. Below we consider possibilities (I) and (II) in more detail. We consider two scenarios for Model II: a model in which the expanding bubbles are driving large-scale shocks into the ISM (Model IIa), and one in which jet/ISM interactions in the inner parts of the outflow are heating the ISM and causing it to be entrained into the bubbles (Model IIb).

5.1. Model I: hot gas from a galactic wind

As NGC 6764 is a galaxy with known starburst activity, the presence of a galactic wind (e.g. Veilleux et al. 2005) producing the observed X-ray emission must be considered. The morphology of the X-ray emission from NGC 6764 is similar to some of the known examples of X-ray-detected galactic winds in nearby galaxies (e.g. Strickland et al. 2004b). For example, the X-ray structures in the starburst galaxies M82 and NGC 1482 have similar opening angles to the bubbles in NGC 6764. In both of these cases the X-ray-emitting gas is coincident with $H\alpha$ filaments extending out of the galaxy disk, which is also the case for NGC 6764 (see Fig. 12 of HS06). However, radio bubbles coincident with the X-ray-emitting gas are not present in either M82 or NGC 1482. We note also that the X-ray morphology of these two systems is not consistent with a uniformly filled sphere or truncated cone, as it is slightly brighter towards the edges rather than in the centre.

NGC 6764 shows strong evidence for circumnuclear starburst activity (e.g. Eckart et al. 1991, 1996; Schinnerer et al. 2000). There is also evidence that the nuclear starburst is producing an outflow: e.g. Leon et al. (2007) estimated, based on CO observations, that $\sim 4 \times 10^6 M_{\odot}$ of molecular gas is outflowing at speeds of $\sim 25 \text{ km s}^{-1}$. However, Eckart

FIG. 5.— Left: Close-up of the X-ray emission from the inner jet/outflow region from the 0.5 - 5.0 keV image smoothed with a Gaussian of $0.6''$ FWHM, with 5-GHz contours overlaid from a map made from archival data as published in Hota & Saikia (2006). Contour levels are $(8.0 \times 10^{-5}) \times 1, 2, 4, \dots, 512$ Jy beam^{-1} ; right: hardness ratio map, as described in the text. White is hard and red is soft. There is a statistically significant increase in hardness to the western edge associated with a region of flatter spectrum radio emission.



et al. (1991) estimated a total star formation rate of $\sim 4 M_{\odot} \text{ yr}^{-1}$, with a supernova rate of $\sim 1.2 \times 10^{-2} \text{ yr}^{-1}$, which is significantly lower than the SFR of $13 - 33 M_{\odot} \text{ yr}^{-1}$ for M82 estimated by Förster Schreiber et al. (2003). The kinetic energies of the outflowing material detected in HI absorption (HS06) and CO emission (Leon et al. 2007) are 8.5×10^{52} ergs and 2.4×10^{53} ergs, respectively, which are both several orders of magnitude below the thermal energy of the X-ray emitting gas. Leon et al. estimated the typical energies available from supernovae and stellar winds given its inferred star formation rate, finding values in the range $10^{54} - 10^{55}$ ergs. It is therefore unclear that sufficient energy is available from starburst activity to power the observed X-ray emission.

The median 0.3 - 2.0 keV X-ray luminosity for galactic winds for the starburst galaxies in the sample of Strickland et al. (2004a, 2004b) is $2.5 \times 10^{39} \text{ erg s}^{-1}$, which is an order of magnitude lower than the X-ray luminosity of the emission from NGC 6764 in the same energy range. The highest luminosity wind in their sample has a 0.3 - 2.0 keV X-ray luminosity of $L_X = 8.3 \times 10^{39} \text{ erg s}^{-1}$, a factor of 2 lower than that of NGC 6764. While NGC 6764 is therefore more luminous than other known galactic winds, its luminosity is not so extreme as to preclude a similar origin. However, the X-ray emission from the bubbles of NGC 6764 (excluding the bright central region) originates from a smaller volume (e.g. the height in kpc above the disk to which the emission extends is a factor of ~ 3 times smaller in NGC 6764 than in M82), hence the volume emissivity is considerably higher.

The diffuse $H\alpha$ emission from NGC 6764 has a total luminosity of $(6 - 8) \times 10^{40} \text{ erg s}^{-1}$ (Zurita et al. 2000), giving a value of $L_X/L_{H\alpha} \sim 3 - 4$. In contrast, the ratio of $L_X/L_{H\alpha}$ for the starburst wind in M82 is ~ 19 (using the $H\alpha$ luminosity measured by McCarthy et al. (1987)). We note also that the “mean” temperatures for the galactic winds in the Strickland et al. sample are typically significantly lower than that of the gas in NGC 6764, although these result from two-temperature fits where the hotter component has temperatures similar to our measured value for NGC 6764. We find no evidence for a cooler component of hot gas in NGC 6764 (in two-temperature fits, the second component tends to higher temperatures of $\sim 1 \text{ keV}$ with no significant improvement in

the fitting statistic).

Another important difference between the X-ray emission in NGC 6764 and galactic winds such as M82 is the sharp decrease in surface brightness at its northern and southern boundaries. Rasmussen et al. (2004) compare the inferred density slopes at the outer boundaries of three starburst winds, M82, NGC 253 and the dwarf galaxy NGC 1800, finding slopes of $\alpha \sim 1$, where $n(r) \propto r^{-\alpha}$. In contrast, NGC 6764 shows an initially flat surface brightness profile (see Fig. 4), dropping steeply at distances between 2 and $5''$ for both the northern and southern bubbles, with a slope that corresponds to $\alpha \sim 2.5$. This is a steeper decrease than would be expected for a freely expanding wind (e.g. Chevalier & Clegg 1985).

The presence of hot, overpressured gas in the inner regions of the galaxy is consistent with the presence of a galactic wind; however, its one-sided structure and East-West orientation may be difficult to reconcile with a galactic wind model. We are not aware of any other galactic wind systems in which a central hot-gas outflow with this type of structure has been observed. An alternative is a photoionized wind that is driven directly by the AGN. Such a model cannot be ruled out on energetic grounds alone: our upper limit on the possible hidden nuclear X-ray luminosity is higher than the energy required to power the bubbles for realistic timescales of bubble inflation (e.g. $10^6 - 10^7$ years). However, as for the starburst-driven wind model, the AGN wind model does not appear consistent with the steep decrease in surface brightness of the X-ray bubbles in NGC 6764. The origin of the radio emission is also unclear in this model, and the E-W orientation of the brighter central outflow may be problematic for an AGN wind explanation.

We conclude that there are important differences between the properties of the X-ray emission and starburst activity of NGC 6764 compared to those of well-studied examples of starburst-driven galactic winds. Most crucially, the close correspondence between extended non-thermal radio emission and X-ray emission is not seen in any of the starburst wind systems. HS06 argue that the lack of such radio bubbles in any galaxies that do not possess an AGN indicates that the bubbles are likely to be powered by the AGN radio jet, although their dynamics and evolution may be affected by the

presence of a galactic wind.

5.2. Model Ia: shock heating by the expanding radio bubbles

The properties of the hot gas associated with the radio bubbles in NGC 6764 are similar to those of the shocked gas associated with the kpc-scale radio lobes of Centaurus A and NGC 3801. The temperatures we measure are similar to those seen in NGC 3801, and the gas densities and pressures are comparable to those measured in the shocked shells of gas surrounding Centaurus A [assuming the thermal interpretation of Kraft et al. (2003)]. However, there is no strong evidence for edge-brightening of the X-ray emission – in fact both the radio and X-ray emission appear to have similar structures, with a slight surface brightness deficit towards the centre of the bubbles, particularly in the north. It would be possible to contrive a shock geometry in which there was more shocked material in front of or behind the bubbles relative to that at the sides, thus counteracting the effect of edge-brightening; however, the smoothness of the X-ray emission argues against a model in which the shocked material is very inhomogeneous.

We first considered the case where the X-ray emission is produced from shocked shells of gas surrounding the radio bubbles. Assuming a strong adiabatic shock, the expected density contrast between shocked and unshocked gas should be a factor of 4. Therefore a shocked gas model requires a surrounding medium with $n_e \sim 0.08 \text{ cm}^{-3}$. As X-ray surface brightness depends primarily on the gas density, we can use an upper limit on the X-ray surface brightness from regions surrounding the X-ray emission associated with the radio bubbles to investigate whether a hot gas medium could be being shocked. We considered a rectangular region covering the eastern half of the southern radio bubble and a matched background region next to the X-ray bright region. We found a surface brightness of $\sim 9.4 \pm 0.1 \text{ net ACIS-S } 0.5 - 5 \text{ keV counts arcsec}^{-2}$ in the source region. If hot gas with a density a factor of 4 lower than that in the bright regions were present, we would expect it to have a surface brightness a factor ~ 16 times lower, e.g. $S_X \sim 0.59 \pm 0.01 \text{ counts arcsec}^{-2}$ (if the unshocked material is cooler this prediction decreases somewhat, e.g. to $0.5 \text{ counts arcsec}^{-2}$ for $kT = 300 \text{ eV}$). We measure an upper limit of $\sim 0.1 \text{ counts arcsec}^{-2}$ from the region external to the southern radio bubble, well below this prediction. It therefore seems unlikely that hot ionized plasma can be the medium being shocked.

The densities of molecular gas in the centre of NGC 6764 are much higher than our prediction for the density of the material being shocked (e.g. $n_e \sim 3 \times 10^3 - 3 \times 10^4 \text{ cm}^{-3}$; Eckart et al. 1991). A possible candidate for material being shocked is the warm, diffuse interstellar medium, which has typical electron densities of $\sim 0.2 \text{ cm}^{-3}$ (e.g. Walterbos 1998). If the bubbles extend perpendicular to the plane of the galaxy disk, then they are likely to be probing regions of lower than average ISM density. In addition, a weaker shock could result in a density contrast lower than 4, and so this candidate for shocked material cannot be ruled out on grounds of density. As seen in Fig. 12 of HS06, the radio bubbles of NGC 6764 are coincident with an extended region of H α -emitting gas (Zurita et al. 2000), with brighter filaments associated with the radio bubbles, indicating that the radio bubbles are likely to be embedded in diffuse gas.

The most likely large-scale shock scenario is one in which a strong shock is propagating into a multiphase medium. We can use the postshock temperature to estimate the shock

speed, assuming that the pre-shocked gas pressure is negligible. The inferred expansion speed is $\sim 740 \text{ km s}^{-1}$, which is comparable to the radio-lobe expansion speeds measured from the shock properties in NGC 3801 ($\sim 850 \text{ km s}^{-1}$), and would imply a total kinetic energy in the shocked material of $\sim 3 \times 10^{55}$ ergs, similar to, but slightly lower than the thermal energy stored in the shells. If the shells are expanding at such a high speed, then the age of the X-ray features must be low ($\sim 10^6$ years, assuming a sound speed appropriate for a hot gas ISM), implying that either the features are short-lived or the gas supply is being replenished. If the latter is the case, then an outflow of gas from the galaxy is likely to be required to supply the ionized gas halo, even if it does not supply the energy to power the X-ray emission.

5.3. Model Ib: Heating by jet/ISM interactions in the central outflow region

The X-ray bright, overpressured region in the central few arcsec of the galaxy suggests a second model for jet-related heating of the X-ray-emitting gas. If this region is an outflow that is supplying material for the large-scale bubbles, then it is clear from the good radio and X-ray correspondence that it contains both hot gas and a population of radio-emitting, non-thermal particles, presumably supplied by a radio jet. The central X-ray/radio morphology is hard to explain in Model Ia, although the X-ray emission could be caused by expansion of the bubbles near to the nucleus. The most plausible explanation for the close correspondence, assuming that the radio plasma traces a nuclear outflow, is that the ISM is being heated and compressed as it interacts with the radio-emitting outflow. The interactions may also be responsible for decollimating the flow. If the radio plasma and heated gas components can become well mixed in the inner outflow, then it seems likely that they will remain mixed on larger scales. Hence an alternative jet-heating scenario is one in which the inner jet is disrupted by interactions with the clumpy ISM, which also heat ISM gas and cause it to be mixed in with the jet fluid. This is similar to the ‘‘frustrated jet’’ model discussed by Gallimore et al. (2006), which predicts soft X-ray emission associated with shocks and entrained material. While the energy is clearly available from the jet to enable such heating on small scales to occur, it is unclear how the details of such a heating and mixing process can work in practice.

In this scenario the bubbles are filled with hot, thermal gas. In this case we would expect significant depolarization of the radio synchrotron emission. Using the radio data discussed above, we found that the integrated fractional polarization of the bubbles is $< 2\%$ and $< 5\%$ at 1.4-GHz and 5-GHz, respectively. This is consistent with the level of expected internal Faraday depolarization given the gas density and equipartition magnetic field strength in the bubbles (see Cioffi & Jones 1980). While the level of polarization is consistent with Model Ib, it is also consistent with an external Faraday screen having the density and path length expected for shocked gas surrounding the bubbles in Model Ia (for reasonable values of the magnetic field strength and plausible assumptions about the cell size in the Faraday screen) using the analysis of Burn (1966), and so we cannot rule out Model Ia on this basis.

The right-hand panel of Fig. 5 shows a hardness ratio map obtained by dividing Gaussian smoothed images in the 1.0 – 5.0 keV and 0.4 – 1.0 keV energy ranges. The region of harder X-ray emission along the western edge of the bubbles is statistically significant (as verified by comparing count ratios with uncertainties for the western and eastern edges of the

bubbles), and corresponds to a region of flatter radio spectral index as shown in HS06. Gallimore et al. (1996) propose a similar explanation for component C of the parsec-scale jet in NGC 1068 parsec-scale jet, which has a similar spectral index to the regions we consider here and is associated with H₂O maser emission. These results suggest that the East-West outflow may be shock heating the ISM in this region, leading to an increase in X-ray temperature, and a flattening of the radio spectrum due to localized particle acceleration. The radio and X-ray spectral structure therefore offer support for a model in which shock heating plays at least some role in heating the X-ray emitting gas. The edge-brightened radio and X-ray structure of the bubbles suggests that shock heating and particle acceleration may also be occurring at the edges of the bubbles (although there is no flattening of the radio spectrum, or hardening of the X-ray spectrum around the eastern edges). Magnetic field compression offers an alternative explanation for the radio structure, but does not explain the close correspondence with the thermal X-ray emission. The surface brightness profiles of the bubbles (Fig. 4) are too steep to be consistent with a uniformly filled sphere of gas, supporting a model in which some compression and possibly shocks are occurring at the edges of the bubbles.

Sutherland & Bicknell (2007) presented simulations of jet/ISM interactions in a non-homogeneous medium that show some similarities with our observations: the radio and X-ray morphologies of the large-scale bubbles in NGC 6764 are somewhat similar to their “energy-driven bubble” phase, with the inner region having a morphology that could be consistent with their initial “flood and channel” phase, which they find persists in the inner regions of the outflow during the energy-driven phase. In their simulations X-ray emission from shocks driven out by the bubbles is also significant. However, the simulations were for much more powerful jets and for initial environmental conditions quite different to those of NGC 6764 (including a static clumpy ISM), Nevertheless they may provide some qualitative support for a jet/ISM interaction interpretation in NGC 6764.

If it is the radio jet and its environmental impact that are the primary explanation for the bubbles, then it is perhaps surprising that the inner jet/outflow is oriented in the East-West direction, not North-South. This can be explained if the jet direction can change on short timescales, perhaps due to the interactions with dense surrounding material in the inner regions. Kharb et al. (2006) proposed such a model for the Seyfert 2 galaxy Markarian 6, which possesses an inner jet nearly perpendicular to its large-scale radio bubbles, concluding that the jet direction changes on timescales of $10^5 - 10^6$ years. The radio and X-ray outflow properties of NGC 6764 are consistent with the picture described by Gallimore et al. (2006) in which jet-ISM interactions in the inner kiloparsec lead to frustration of the AGN jet. We conclude that this model is somewhat more plausible than a large-scale radio-bubble driven shock (Model IIa); however, neither model can be ruled out.

5.4. Comparisons with other Seyfert radio-bubble systems

HS06 presented a list of Seyfert radio-bubble systems similar to NGC 6764. *Chandra* X-ray studies of three of these systems are published in the literature, NGC 1068, M51 and NGC 3079. Below we discuss the similarities and differences between NGC 6764 and each of these previously studied radio-bubble systems.

The Seyfert 2 galaxy NGC 1068 has two asymmetric ra-

dio bubbles with a total extent of ~ 1 kpc, which are connected to a radio-bright nucleus. The *Chandra* study of Young et al. (2001) showed the presence of bright extended X-ray emission associated with the north-eastern radio bubble, with a lack of corresponding emission associated with the south-western bubble (likely to be due to high absorption from the disk of the galaxy). The X-ray and radio morphology of this system are consistent with similar behaviour to NGC 6764. Young et al. required more complex spectral models to account for the X-ray emission associated with the north-east radio bubble region; however, they were able to obtain spectra of much higher signal-to-noise than ours for NGC 6764, and so it is possible that a single-temperature *mekal* model would also prove inadequate if we were able to obtain similar quality data for NGC 6764. Young et al. suggest that compression of the ISM by the radio ejecta is responsible for the bubble-related X-ray emission.

Terashima & Wilson (2001) presented a *Chandra* study of the extended emission from the Seyfert 2 galaxy M51, which possesses a highly asymmetric two-sided radio bubble structure. As for NGC 6764, they found extended X-ray emission corresponding closely to the radio structure. The X-ray emission is spectrally similar to that seen in NGC 6764 ($kT \sim 0.5 - 0.6$ keV), and interestingly a region of harder X-ray emission is seen at the position where the radio jet is seen to terminate, similar to what is seen in NGC 6764. Terashima & Wilson adopt a shock heating model for M51, finding bubble expansion velocities very similar to those inferred above for NGC 6764 (~ 700 km s⁻¹).

NGC 3079 is another complex starburst/AGN system, which possesses two kpc-scale radio bubble structures. Although the radio structures have been modelled as originating in a nuclear wind (e.g. Duric & Seaquist 1988), long-term VLBI monitoring shows emitting regions whose structure and time variability is consistent with the expectation for a jet interacting with a dense and clumpy surrounding medium (Middelberg et al. 2007). Middelberg et al. also argue that these interactions can explain the large-scale morphology of the radio bubbles. Cecil et al. (2002) present *Chandra* observations of NGC 3079, which show filamentary X-ray structure coinciding with H α filaments; however, there is also a region of X-ray emission associated with the southern radio bubble, which is too faint for spectral analysis. The optical and X-ray filaments to the north do not coincide with the radio bubble, but Cecil et al. claim that there is some evidence for shock heating of gas surrounding the VLBI jet. It is clear that starburst winds are responsible for some of the X-ray structure in NGC 3079, but it remains possible that X-ray emission heated by the expanding radio plasma is also present. The relationship between the radio structure and the optical and X-ray filaments in NGC 3079 is unclear.

Based on the comparisons above, it seems likely that the radio/X-ray bubbles observed in NGC 6764, NGC 1068 and M51 are examples of the same phenomenon, whereas the situation in NGC 3079 may be more complex. We conclude that the behaviour seen in NGC 6764 may be widespread in the Seyfert population, as such outbursts are likely to be short-lived. We would expect similar X-ray properties for radio bubbles in Seyfert 1 galaxies; however, due to the small size scales of the lobes and the expected projection, bubble-related X-ray emission is likely to be difficult to disentangle from the brighter nuclear X-ray emission in these systems.

6. CONCLUSIONS

We have identified X-ray counterparts to the kpc-scale radio bubbles in the Seyfert galaxy NGC 6764, whose morphology traces very closely the radio structures. The energy input from these hot gas features is $\sim 10^{56}$ ergs, comparable to the energy input from shock heating in the low-power radio galaxy NGC 3801. The inferred rate of energy input in NGC 6764 is $\sim 10^{42}$ erg s $^{-1}$, and is expected to have a significant impact on the galaxy and its surroundings. Based on the presence of an inner outflow that appears to emanate from the Seyfert nucleus, seen in both radio and X-ray emission, similarities to X-ray features in previously studied AGN-jet systems, key differences compared to starburst outflows, and the spatial coincidence of a region of flatter radio spectrum and hard X-ray spectrum, suggesting particle acceleration, we conclude that the thermal emission is produced by heating of the ISM due to compression and shocks caused by the AGN

outflow. The morphology of the radio outflow in NGC 6764 leads us to favour a model in which jet/ISM interactions in the inner part of the galaxy lead to heating of the gas and its entrainment into the bubbles, as well as jet disruption; however, we cannot rule out a model in which the bubbles are driving large-scale shocks into the ISM. The existence of a population of kpc-scale radio lobe sources in Seyfert galaxies (expected to be short-lived) suggests that AGN-jet or AGN-jet+starburst powered galaxy feedback as seen in NGC 6764 could be important for the galaxy population as a whole.

We thank the referee for helpful comments. We gratefully acknowledge support from the Royal Society (research fellowship for MJH). This work was partially supported by NASA grant G08-9108X.

REFERENCES

- Awaki, H., Ueno, S., Taniguchi, Y., Weaver, K.A., 2000, *ApJ*, 542, 175
 Baum, S.A., O’Dea, C.P., Dallacassa, D., de Bruyn, A.G., Pedlar, A., 1993, *ApJ*, 419, 553
 Bower, R.G., Benson, A.J., Malbon, R., Helly, J.C., Frenk, C.S., Baugh, C.M., Cole, S., Lacey, C.G., 2006, *MNRAS*, 370, 645
 Buote, D., 2000, *MNRAS*, 311, 176
 Burn, B.J., 1966, *MNRAS*, 133, 67
 Capetti, A., Axon, D.J., Macchetto, F.D., Marconi, A., Winge, C., *ApJ*, 516, 187
 Cecil, G., Bland-Hawthorn, J., Veilleux, S., 2002, *ApJ*, 576, 745
 Chevalier, R.A., Clegg, A.W., 1985, *Nature*, 317, 44
 Cioffi, D.F., Jones, T.W., 1980, *AJ*, 85, 368
 Clements, I., 1981, *MNRAS*, 197, 829
 Croton, D.J. et al. 2006, *MNRAS*, 365, 11
 Croston, J.H., Kraft, R.P., Hardcastle, M.J., 2007, *ApJ*, 660, 191
 Croston, J.H., Hardcastle, M.J., Birkinshaw, M., Worrall, D.M., Laing, R.A., 2008, *MNRAS*, in press (arXiv:0802.4297)
 Dickey, J.M., Lockman, F.J., 1990, *ARA&A*, 28, 215
 Duric, N., Seaquist, E.R., 1988, *ApJ*, 326, 574
 Eckart, A., Cameron, M., Jackson, J.M., Genzel, R., Harris, A.I., Wild, W., Zinnecker, H., 1991, *ApJ*, 372, 67
 Eckart, A., Cameron, M., Boller, Th., Krabbe, A., Blietz, M., Nakai, N., Wagner, S.J., Sternberg, A., 1996, *ApJ*, 472, 599
 Fabian, A.C., Sanders, J.S., Allen, S.W., Crawford, C.S., Iwasawa, K., Johnstone, R.M., Schmidt, R.W., Talor, G.B., 2003, *MNRAS*, 344, L43
 Forman, W. et al. 2005, *ApJ*, 635, 894
 Förster Schreiber, N.M., Genzel, R., Lutz, D., Sternberg, A., 2003, *ApJ*, 599, 193
 Gallimore, J.F., Baum, S.A., O’Dea, C.P., Pedlar, A., 1996, *ApJ*, 458, 136
 Gallimore, J.F., Baum, S.A., O’Dea, C.P., 2004, *ApJ*, 613, 794
 Gallimore, J.F., Axon, D.J., O’Dea, C.P., Baum, S.A., Pedlar, A., 2006, *AJ*, 132, 546
 Hota, A., Saikia, D.J., 2006, *MNRAS*, 371, 945 [HS06]
 Kharb, P., O’Dea, C.P., Baum, S.A., Colbert, E.J.M., Xu, C., 2006, *ApJ*, 652, 177
 Kraft, R.P., Vázquez, S.E., Forman, W.R., Jones, C., Murray, S.S., Hardcastle, M.J., Worrall, D.M., Churazov, E., 2003, *ApJ*, 592, 129
 Kraft, R.P., et al., 2007, *ApJ*, 665, 1129
 Leon, S. et al., 2007, *A&A*, 473, 747
 Matsumoto, C., Nava, A., Maddox, L.A., Leighly, K.M., Grupe, D., Awaki, H., Ueno, S., 2004, *ApJ*, 617, 930
 Matt, G., Bianchi, S., Guainazzi, M., Molendi, S., 2004, *A&A*, 414, 155
 Middelberg, E., Agudo, I., Roy, A.L., Krichbaum, T.P., 2007, *MNRAS*, 377, 731
 McCarthy, P.J., van Breugel, W., Heckman, T., 1987, *AJ*, 93, 264
 Rasmussen, J., Stevens, I.R., Ponman, T.J., 2004, *MNRAS*, 354, 259
 Schinnerer, E., Eckart, A., Boller, Th., 2000, *ApJ*, 545, 205
 Strickland, D.K., Heckman, T.M., Colbert, E.J.M., Hoopes, C.G., Weaver, K., 2004a, *ApJSS*, 151, 193
 Strickland, D.K., Heckman, T.M., Colbert, E.J.M., Hoopes, C.G., Weaver, K., 2004b, *ApJ*, 606, 829
 Sutherland, R.S., Bicknell, G.V., 2007, *Ap&SS*, 311, 293
 Terashima, Y., Wilson, A.S., 2001, *ApJ*, 560, 139
 Walterbos, R.A.M., 1998, *PASA*, 15, 99
 Young, A.J., Wilson, A.S., Shopbell, P.L., 2001, *ApJ*, 556, 6
 Zurita, A., Rozas, M., Beckman, J.E., 2000, *A&A*, 363, 9